

# An Empirical Study on MC Dropout-Based Uncertainty–Error Correlation in 2D Brain Tumor Segmentation

Saumya B

*Project Associate*

*DESE, Indian Institute of Science*

Bengaluru, India

[saumya.b@fsid-iisc.in](mailto:saumya.b@fsid-iisc.in)

**Abstract**—Accurate brain tumor segmentation from MRI is vital for diagnosis and treatment planning. Although Monte Carlo (MC) Dropout is widely used to estimate model uncertainty, its effectiveness in identifying segmentation errors—especially near tumor boundaries—remains unclear. This study empirically examines the relationship between MC Dropout-based uncertainty and segmentation error in 2D brain tumor MRI segmentation using a U-Net trained under four augmentation settings: none, horizontal flip, rotation, and scaling. Uncertainty was computed from 50 stochastic forward passes and correlated with pixel-wise errors using Pearson and Spearman coefficients. Results show weak global correlations ( $r \approx 0.30\text{--}0.38$ ) and negligible boundary correlations ( $|r| < 0.05$ ). Although differences across augmentations were statistically significant ( $p < 0.001$ ), they lacked practical relevance. These findings suggest that MC Dropout uncertainty provides limited cues for boundary error localization, underscoring the need for alternative or hybrid uncertainty estimation methods in medical image segmentation.

**Index Terms**—Brain tumor segmentation, uncertainty–error correlation, boundary uncertainty, Monte-Carlo dropout

## I. INTRODUCTION

Accurate segmentation of brain tumors in magnetic resonance imaging (MRI) is essential for diagnosis, treatment planning, and monitoring disease progression. Deep learning models, particularly convolutional neural networks such as U-Net, have demonstrated remarkable success in automating tumor segmentation. Although most recent research focuses on 3D brain tumor segmentation, 2D segmentation remains important for computationally efficient pipelines, preliminary analyses, and educational purposes. Despite these advances, segmentation models are prone to errors, especially near tumor boundaries, where irregular shapes and low contrast make precise delineation challenging. Investigating uncertainty estimation in 2D segmentation offers valuable insights into model behavior and error localization, with implications that extend to both 2D and 3D segmentation tasks.

Uncertainty estimation has been proposed as a means to identify regions where the model’s predictions may be unreliable, with the potential to guide clinicians in reviewing or refining the segmentation output. Monte Carlo (MC) Dropout is a widely used technique for estimating model uncertainty

by leveraging dropout layers during inference to generate multiple stochastic forward passes. The resulting variance across predictions is interpreted as model uncertainty.

In this report, we investigate the relationship between MC Dropout uncertainty and segmentation errors in the context of 2D brain tumor segmentation. Specifically, we explore whether uncertainty estimates can effectively highlight error-prone regions at tumor boundaries, which are critical areas for clinical decision-making. We further evaluate this relationship under different data augmentation settings to assess the robustness of uncertainty estimates and perform statistical analyses to determine the significance and practical relevance of observed correlations.

The major contributions of this work are given below:

- (i) We quantify the correlation between uncertainty and segmentation error at both global and boundary levels in 2D brain tumor MRI segmentation
- (ii) We analyze the effect of data augmentation on uncertainty–error relationships, and
- (iii) We perform statistical tests to assess the robustness and significance of these correlations

## II. LITERATURE SURVEY

In recent years, there has been increasing interest in developing trustworthy AI systems that incorporate explainability, robustness, and accountability principles to ensure that automated predictions are interpretable and reliable in clinical settings [1], [2]. In particular, uncertainty estimation has been proposed as a tool to complement segmentation predictions by allowing clinicians to identify regions where the model’s confidence is low. When uncertainty is high, clinicians can integrate additional diagnostic tests, patient history, or manual review to mitigate potential errors. Uncertainty estimation in deep learning is broadly classified into epistemic uncertainty, which arises from limited knowledge about the model or data distribution, and aleatoric uncertainty, which stems from inherent noise in the data [3]. Epistemic uncertainty can be modelled through Bayesian frameworks or ensembles of mod-

els and is theoretically reducible with more data or improved model structure.

Uncertainty estimation in medical image analysis has been comprehensively reviewed by Zou et al. (2022) [4], who classified approaches into Bayesian and non-Bayesian categories and discussed their applications in segmentation, detection, and classification tasks. Among these, Monte Carlo (MC) Dropout [5] has become one of the most widely adopted techniques, serving as an efficient approximation to Bayesian neural networks. By enabling dropout at inference, MC Dropout generates multiple stochastic predictions and estimates uncertainty with minimal additional computational cost [6], [7]. Numerous studies have extended MC Dropout for medical imaging tasks, including lesion detection and segmentation of polyps, as well as semi-supervised learning in cardiac and neuroimaging domains [8]–[10].

However, despite its popularity, MC Dropout has been shown to suffer from several limitations. Recent studies have highlighted that uncertainty estimation methods, including MC Dropout, are poorly calibrated at finer scales and may fail to highlight error-prone regions reliably. Fuchs et al. (2022) [11] demonstrated that MC Dropout produced poorly calibrated uncertainty maps in brain tumor segmentation, especially near boundaries where errors are most likely. Similarly, Mehrtash et al. (2020) [12] found that MC Dropout’s calibration improvements were inconsistent across datasets and inferior to ensemble methods in both calibration and out-of-distribution detection. These findings suggest that dropout-based uncertainty estimation may not be sufficient for practical error localization in medical imaging.

Despite existing work highlighting the limitations of MC Dropout in uncertainty estimation for brain tumor segmentation, these studies have primarily relied on dataset-level metrics such as calibration errors or visual uncertainty maps, and have focused largely on volumetric (3D) data. To the best of our knowledge, there is no systematic investigation quantifying the relationship between uncertainty and segmentation error at the per-image or boundary level in 2D segmentation tasks. Specifically, statistical analyses such as Pearson correlation and Spearman correlation between uncertainty and error, or paired t-tests comparing different augmentation settings, have not been employed to rigorously evaluate the practical utility of MC Dropout for boundary error localization. This study addresses that gap by providing a detailed, image-wise uncertainty-error analysis in 2D brain tumor segmentation under various augmentation scenarios.

### III. METHODOLOGY

All experiments were conducted on a single NVIDIA T4 GPU in Google Colab with memory growth enabled to prevent full GPU memory pre-allocation. Training used `tf.distribute.MirroredStrategy`, which defaults to a single device in this environment and does not affect determinism. To control randomness, we fixed seeds for Python, NumPy, and TensorFlow, but did not enforce deterministic cuDNN kernels;

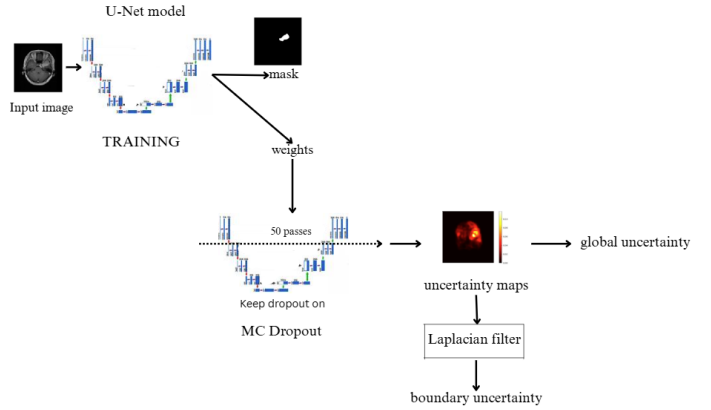


Fig. 1. Workflow diagram

thus, exact bit-wise reproducibility is not guaranteed. The global batch size was set to 8.

The primary objective of this study was to investigate how the uncertainty correlation with segmentation error changes across different data augmentation strategies. We trained a standard U-Net architecture using four augmentation settings—horizontal flipping, rotation, scaling, and no augmentation—evaluated independently. Although segmentation metrics such as precision, recall, and Intersection over Union (IoU) were computed to describe model performance, the main focus was on analyzing the relationship between uncertainty and error.

The trained weights from each model were then used to perform Monte Carlo (MC) dropout-based uncertainty estimation. For each augmentation setting, inference was run 50 times with dropout enabled, and the variance across the predictions was computed as a measure of epistemic uncertainty. Pixel-wise uncertainty was then correlated with segmentation error to assess how well uncertainty reflects inaccuracies under different augmentation techniques. This framework enabled a direct comparison of uncertainty–error relationships across augmentation strategies, when uncertainty was quantified using MC dropout.

#### A. Dataset

For this study, a brain tumor dataset containing 3064 T1-weighted contrast-enhanced MRI images was used. The dataset originates from the work of Jun Cheng, who collected them from Nanfang Hospital and Tianjin Medical University in China, between 2005 and 2010 [13], [14]. The dataset comprises images from 233 patients and includes 708 cases of meningioma, 1426 cases of glioma, and 930 cases of pituitary tumors. According to the original source, tumor boundaries were manually annotated by three experienced radiologists. While the original dataset is hosted on Figshare, we used a version available on Kaggle [15], where the scans and corresponding binary masks were provided as 2D images of dimension 256×256 pixels. To assess class imbalance, we estimated the proportion of tumor-labelled pixels in the training masks. Over 100 randomly sampled training batches,

tumor pixels comprised approximately 1.66% of all pixels, confirming strong class imbalance.

### B. Preprocessing

The image–mask pairs from the dataset were first converted to grayscale and resized to a fixed dimension of 256×256 pixels. Bilinear interpolation was used for resizing the images, while nearest-neighbor interpolation was applied to the tumor segmentation masks. The latter preserves the discrete 0/1 label values and avoids introducing gray pixels at the boundaries, which can occur with bilinear interpolation.

The images and masks were then converted to NumPy arrays and normalized by dividing by 255. The image–masks were then cast to `tf.float32`. Optional data augmentation was applied on-the-fly during training. Four augmentation settings were studied individually: no augmentation (baseline), horizontal flip, rotation, and scaling. The details of each augmentation settings are summarized in Table 1.

The dataset was split into training, validation, and test sets in a 60:20:20 ratio. To ensure consistency and prevent data leakage across experiments, the same splits were used for all augmentation settings. Images were first sorted and then split using a fixed random seed (seed = 42) in each notebook. As the image–mask pairs remained in the same order and the splitting process was deterministic, the resulting datasets were identical across all experiments, eliminating dataset variability. This ensures that any observed differences in model performance or uncertainty–error relationships are attributable solely to the augmentation methods, rather than variations in the dataset splits.

TABLE I  
DETAILS OF DATA AUGMENTATION TECHNIQUES APPLIED

Technique	% of training dataset	Parameters
Horizontal Flip	50%	none
Rotation	50%	Angle: $\pm 15^\circ$
Random Scaling	50%	Range: 0.8 - 1.2

### C. Model Architecture

We adopted the classic U-Net architecture (Ronneberger et al., 2015) [16] as the baseline model for tumor segmentation. The encoder–decoder structure with skip connections was retained without major modifications; hence, the architecture can be considered a vanilla U-Net. Each convolutional block consisted of two convolutional layers with ReLU activation, followed by max pooling in the encoder and transposed convolutions in the decoder. To adapt the model to our task, we introduced dropout layers after each pooling and upsampling operation (to enable Monte Carlo Dropout uncertainty estimation) and employed Focal Loss (Lin et al., 2017) [17] instead of the conventional cross-entropy, to address the strong class imbalance observed in the dataset. This loss function downweights easy background pixels and emphasises hard examples near the tumor boundary. The final layer was a 1×1 convolution with sigmoid activation, producing a binary

segmentation mask. The network had approximately 34.5M trainable parameters.

The U-Net model was trained using the Adam optimizer (learning rate=  $1 \times 10^{-4}$ ) with focal loss as the loss function. Accuracy, precision, and recall were monitored as evaluation metrics during training. Because of the nature of the task at hand, accuracy metric obtained was ignored and instead emphasis was placed on precision and recall metrics. To address class imbalance and emphasize correct tumor detection, the validation recall metric was used for early stopping (patience = 7, min delta = 0.005). Training was capped at 70 epochs, and the model weights corresponding to the best validation recall were restored for final evaluation. The model with the best validation recall was restored using the early stopping callback; intermediate checkpointing was omitted to reduce training overhead. During training, we monitored loss, precision, and recall for both training and validation sets. These metrics were plotted together as training curves and archived for each run. Hyperparameters, metrics and training curves were logged for each run and can be found in the author’s GitHub repository. After training, segmentation performance was evaluated quantitatively using the metrics described below.

TABLE II  
MODEL HYPERPARAMETERS AND TRAINING CONFIGURATION

Category	Hyperparameter	Value
Model Architecture	Input Shape	(256, 256, 1)
	Kernel Size (Initial)	(3, 3)
	Kernel Size (Subsequent)	(3, 3)
	Activation function	ReLU
	Kernel Initializer	He Normal
	Dropout Rate	0.3
	Final Activation	Sigmoid
Loss and Metrics	Loss function	Focal Loss
	Optimizer	Adam
	Training metrics	Accuracy
Training Parameters	Batch Size	8
	Learning Rate	$1 \times 10^{-4}$
	No. of epochs	70

### D. Metrics for evaluating segmentation accuracy

Segmentation quality was evaluated using both per-image and global metrics.

1) *Intersection-over-Union (IoU)*: Per-image segmentation performance was quantified using the Intersection-over-Union (IoU) metric over the test set. To avoid division by zero in cases where both ground-truth and predicted masks contained no positive pixels, a small constant ( $\varepsilon = 1 \times 10^{-6}$ ) was added to both numerator and denominator.

$$IoU = \frac{TP + \varepsilon}{TP + FP + FN + \varepsilon} \quad (1)$$

Where TP, FP and FN denote the number of true positive, false positive, and false negative pixels, respectively, and  $\varepsilon = 1 \times 10^{-6}$  prevents division by zero.

2) *Precision and Recall*: Pixel-level performance was further assessed using precision and recall, defined as:

$$\text{Precision} = \frac{TP}{TP + FP + \varepsilon}, \quad \text{Recall} = \frac{TP}{TP + FN + \varepsilon} \quad (2)$$

where TP, FP, and FN denote the number of true positive, false positive, and false negative pixels, respectively, and  $\varepsilon = 1 \times 10^{-6}$  prevents division by zero. During training, global precision and recall were monitored using `tf.keras.metrics`, while post-training evaluation employed the per-image mean IoU and its standard deviation. Uncertainty maps generated via Monte Carlo Dropout were further analyzed to examine correlations between predicted uncertainty and segmentation errors.

#### E. Uncertainty Estimation

To quantify model confidence in segmentation predictions, Monte Carlo (MC) Dropout [5] was employed at inference. Dropout layers, introduced after each encoder and decoder block of the U-Net, were activated during test time to perform  $T = 50$  stochastic forward passes per image. For each pixel, the mean prediction across these passes was used as the final segmentation probability, while the standard deviation served as a measure of epistemic uncertainty. Two complementary approaches were used to analyze uncertainty:

##### 1) Overall (total) uncertainty:

- For each image, the mean of the per-pixel uncertainty map was computed, yielding a single scalar representing the overall model uncertainty for the image.
- This metric captures the general confidence of the model across the entire image.

##### 2) Boundary-specific uncertainty:

- Tumor boundaries were extracted from the predicted binary mask using a Laplacian edge detection filter.
- Uncertainty values at the boundary pixels were then analyzed to compute:
  - Mean boundary uncertainty
  - Standard deviation of boundary uncertainty
  - Maximum boundary uncertainty
  - Boundary length (number of boundary pixels)
- These metrics specifically capture uncertainty in regions most prone to segmentation errors, as errors are typically concentrated along tumor edges.

The resulting uncertainty metrics were stored per image and later used for correlation analysis with segmentation errors.

#### F. Uncertainty - Error Correlation

To investigate whether regions of high model uncertainty correspond to actual segmentation errors, we first generated per-pixel error maps by thresholding the predicted probability maps at 0.5 and comparing the resulting binary masks against the ground truth. Pixels where prediction and ground truth disagreed were marked as errors. We then quantified the relationship between model uncertainty and these error maps using both Pearson correlation coefficients (to assess linear dependence) and Spearman rank correlations (to capture

monotonic but potentially non-linear relationships). For each test image, the per-pixel uncertainty and error maps were flattened, and correlations were computed independently. To specifically assess performance at tumor interfaces (regions that are particularly error-prone), we repeated the analysis by restricting pixels to those lying along the predicted tumor boundaries, identified using a Laplacian-based edge filter. This enabled a focused evaluation of whether uncertainty estimates provide meaningful cues for boundary error localization, beyond global correlations across the entire image.

Furthermore, to assess whether differences in uncertainty–error correlations across augmentation settings were statistically significant, we conducted paired statistical tests on the per-image correlation values. Specifically, we applied the paired t-test to compare mean correlations, and the Wilcoxon signed-rank test as a non-parametric alternative that does not assume normality of the differences. This dual approach ensured that our conclusions regarding statistical significance were robust to distributional assumptions.

## IV. RESULTS AND DISCUSSION

### A. Segmentation Performance

The segmentation performance across different augmentations is provided in Table 3. As seen in the table, the performance is fairly stable across different augmentations.

TABLE III  
SEGMENTATION PERFORMANCE ACROSS DIFFERENT AUGMENTATION  
TECHNIQUES

Augmentation type	Global Precision	Global Recall	Per image mean IoU
No augmentation	0.856	0.779	$0.6910 \pm 0.2633$
Horizontal Flip	0.875	0.713	$0.6338 \pm 0.2883$
Rotation	0.871	0.736	$0.6556 \pm 0.2783$
Scaling	0.884	0.742	$0.6730 \pm 0.2802$

### B. Uncertainty Analysis

The results from the uncertainty analysis across different augmentations are mentioned in Table 4. As seen in Table 4, scaling showed the least mean total uncertainty value. To further interpret model confidence, we generated per-image visualizations including predicted masks and per-pixel uncertainty maps. For clarity in the heatmap, a Gaussian filter ( $\sigma = 1$ ) was applied to the per-pixel uncertainty maps. This smoothing was used only for visualization purposes; all quantitative analyses, including uncertainty metrics and correlation with segmentation errors, were computed on the raw, unsmoothed uncertainty values. These visualizations, as shown in Figure 2, show that the predicted uncertainty for the same input image across different augmentation settings shows visible differences. While there was visual difference between uncertainty maps, quantitative correlation with error remained low and constant across different augmentations, as shown in subsection IV (C). This indicates that per-image uncertainty maps obtained are not reliable indicators of error-prone regions.

TABLE IV  
RESULTS FROM UNCERTAINTY ANALYSIS ACROSS DIFFERENT AUGMENTATION SETTINGS

Augmentation type	Average Total uncertainty	Mean boundary uncertainty	Max boundary uncertainty	Std boundary uncertainty
No augmentation	0.0034	0.0590	0.1089	0.0192
Horizontal flip	0.0044	0.0382	0.0656	0.0101
Rotation	0.0041	0.0457	0.0763	0.0117
Scaling	0.0027	0.0549	0.0985	0.0167

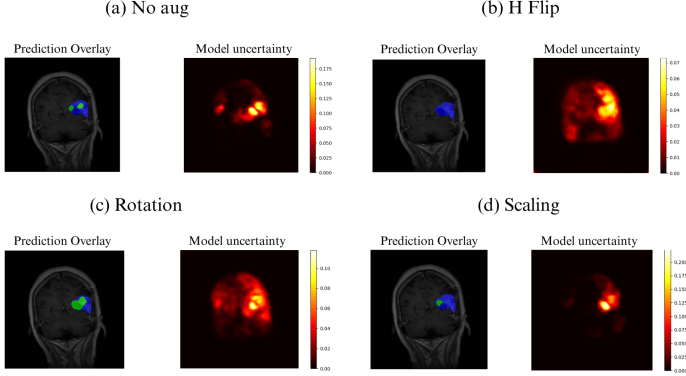


Fig. 2. Predicted segmentation mask and uncertainty maps across different settings (Green = Predicted mask, Blue = Ground truth); Visual comparison shows visible differences in uncertainty maps between augmentations

### C. Uncertainty-Error Correlation

To evaluate how well model uncertainty reflected segmentation inaccuracies, we computed both Pearson’s correlation coefficient ( $r$ ) and Spearman’s rank correlation ( $\rho$ ) between per-image uncertainty measures and segmentation errors, under each augmentation setting. Table 6 summarizes the correlation values.

(a) Global correlation :Across all four settings, global correlations were modest: Pearson  $r$  ranged from 0.30 to 0.37. Scaling produced the highest correlation (0.3781), while horizontal flip yielded the lowest (0.3014). Spearman correlation values were generally lower, ranging between 0.1115 and 0.1198, indicating weak monotonic relationships. Although pairwise t-tests on the global correlation distributions yielded  $p < 0.05$ , the absolute differences between settings were small ( $< 0.07$ ). This indicates that while the differences are statistically detectable, they are unlikely to be of practical significance.

(b) Boundary correlation: At the tumor boundary, Pearson correlations were close to zero, ranging between  $-0.0006$  and 0.0458, while Spearman correlations similarly hovered around zero, between  $-0.0054$  and 0.0453. This suggests that uncertainty at boundary regions had little to no association with segmentation error.

Table 5 presents the pairwise comparison of mean uncertainty-error correlations between the baseline (no augmentation) and each augmentation setting. Although the absolute differences in mean correlation ( $\Delta$ Mean) were small ( $< 0.05$ ), both the paired t-test and Wilcoxon signed-rank test yielded

highly significant p-values ( $p < 0.001$ ) for all comparisons. This indicates that while augmentation-induced differences are statistically detectable due to the size and consistency of the test set, their magnitude is negligible, suggesting limited practical significance. Overall, the results indicate that global uncertainty exhibits only weak correlation with segmentation error, while boundary uncertainty provides little to no additional information for error prediction. Moreover, the minimal variation across augmentation settings highlights that data augmentation has limited influence on the uncertainty-error relationship in this 2D brain tumor segmentation task.

### D. Discussion

The analysis indicates that MC Dropout uncertainty correlates weakly with segmentation error in the context of 2D brain tumor segmentation, particularly at tumor boundaries where uncertainty is expected to reflect error-prone regions. While global uncertainty metrics showed modest correlations (Pearson  $r$  ranging from 0.3014 to 0.3781), boundary correlations were negligible ( $|r| < 0.05$ ), suggesting that uncertainty estimates from MC Dropout do not reliably highlight regions with segmentation errors.

Although pairwise t-tests on the global correlation distributions yielded  $p < 0.05$ , the absolute differences between settings were small ( $< 0.07$ ), implying that the differences are statistically detectable but unlikely to be of practical significance. This further reinforces the notion that augmentation variations do not meaningfully affect the relationship between uncertainty and error in this setup.

It is important to note that these findings are specific to the task studied—2D brain tumor segmentation using a U-Net architecture with MC Dropout. The results should not be generalized to other segmentation tasks, data modalities, or uncertainty estimation techniques. However, within this experimental setup, MC Dropout appears to be insufficient for boundary refinement or error localization based on uncertainty measures alone.

## V. CONCLUSION AND FUTURE SCOPE

In this work, we evaluated the suitability of MC Dropout uncertainty for identifying segmentation errors in 2D brain tumor segmentation, and the effect of augmentation on such correlations. The results demonstrate weak global correlations and negligible boundary-level correlations between uncertainty and error, despite statistical significance across augmentation settings. These findings suggest that, for this particular

TABLE V  
STATISTICAL TESTS ON MEAN UNCERTAINTY–ERROR CORRELATIONS BETWEEN AUGMENTATION CONDITIONS

Comparison	Mean Overall Corr (A)	Mean Overall Corr (B)	$\Delta$ Mean	p-value (t-test)	p-value (Wilcoxon)
No aug v/s horizontal flip	0.3365	0.3014	0.0351	$1.4220 \times 10^{-10}$	$2.1080 \times 10^{-12}$
No aug v/s rotation	0.3365	0.3106	0.0259	$1.4603 \times 10^{-6}$	$8.4130 \times 10^{-7}$
No aug v/s scaling	0.3365	0.3781	-0.0416	$4.6668 \times 10^{-14}$	$9.3600 \times 10^{-21}$

TABLE VI  
PEARSON AND SPEARMAN RANK CORRELATION TABLE

Augmentation type	Pearson $r$		Spearman $\rho$	
	Global	Boundary	Global	Boundary
No augmentation	0.3365	-0.0006	0.1115	-0.0054
Horizontal flip	0.3014	0.0369	0.1198	0.0349
Rotation	0.3106	0.0458	0.1171	0.0453
Scaling	0.3781	0.0195	0.1136	0.0171

task and model, MC Dropout is not a suitable method for uncertainty-based boundary correction or error localization. Augmentation techniques do not significantly improve the uncertainty-error correlation in this context. Future studies may explore alternative uncertainty estimation techniques or task-specific adaptations to better capture segmentation errors, particularly at boundaries. Additionally, extending this analysis to other datasets and architectures will help clarify the broader applicability of uncertainty-driven methods in medical image segmentation.

**Data and code availability:** All code and experimental configurations are publicly available at <https://github.com/Saumya4321/mc-dropout-boundary-correlation>.

## REFERENCES

- [1] Li, B., Qi, P., Liu, B., Di, S., Liu, J., Pei, J., Yi, J. and Zhou, B., 2023. Trustworthy AI: From principles to practices. ACM Computing Surveys, 55(9), pp.1-46.
- [2] Liang, W., Tadesse, G.A., Ho, D., Fei-Fei, L., Zaharia, M., Zhang, C. and Zou, J., 2022. Advances, challenges and opportunities in creating data for trustworthy AI. Nature Machine Intelligence, 4(8), pp.669-677.
- [3] Der Kiureghian, A. and Ditlevsen, O., 2009. Aleatory or epistemic? Does it matter?. Structural safety, 31(2), pp.105-112.
- [4] Zou, K., Chen, Z., Yuan, X., Shen, X., Wang, M. and Fu, H., 2023. A review of uncertainty estimation and its application in medical imaging. Meta-Radiology, 1(1), p.100003.
- [5] Gal, Y. and Ghahramani, Z., 2016, June. Dropout as a Bayesian approximation: Representing model uncertainty in deep learning. In International Conference on machine learning (pp. 1050-1059). PMLR.
- [6] Srivastava, N., Hinton, G., Krizhevsky, A., Sutskever, I. and Salakhutdinov, R., 2014. Dropout: a simple way to prevent neural networks from overfitting. The Journal of machine learning research, 15(1), pp.1929-1958.
- [7] Lakshminarayanan, B., Pritzel, A. and Blundell, C., 2017. Simple and scalable predictive uncertainty estimation using deep ensembles. Advances in neural information processing systems, 30.
- [8] Nair, T., Precup, D., Arnold, D.L. and Arbel, T., 2020. Exploring uncertainty measures in deep networks for multiple sclerosis lesion detection and segmentation. Medical image analysis, 59, p.101557.
- [9] Wickstrøm, K., Kampffmeyer, M. and Jenssen, R., 2020. Uncertainty and interpretability in convolutional neural networks for semantic segmentation of colorectal polyps. Medical image analysis, 60, p.101619.
- [10] Yu, L., Wang, S., Li, X., Fu, C.W. and Heng, P.A., 2019, October. Uncertainty-aware soft-ensembling model for semi-supervised 3D left atrium segmentation. In International Conference on Medical Image Computing and Computer-Assisted Intervention (pp. 605-613). Cham: Springer International Publishing.
- [11] Fuchs, M., Gonzalez, C. and Mukhopadhyay, A., 2021. Practical uncertainty quantification for brain tumor segmentation. In Medical Imaging with Deep Learning.
- [12] Mehrtash, A., Wells, W.M., Tempany, C.M., Abolmaesumi, P. and Kapur, T., 2020. Confidence calibration and predictive uncertainty estimation for deep medical image segmentation. IEEE transactions on medical imaging, 39(12), pp.3868-3878.
- [13] Cheng, J., Huang, W., Cao, S., Yang, R., Yang, W., Yun, Z., Wang, Z. and Feng, Q., 2015. Enhanced performance of brain tumor classification via tumor region augmentation and partition. PloS one, 10(10), p.e0140381
- [14] Cheng, J., Yang, W., Huang, M., Huang, W., Jiang, J., Zhou, Y., Yang, R., Zhao, J., Feng, Y., Feng, Q. and Chen, W., 2016. Retrieval of brain tumors by adaptive spatial pooling and Fisher vector representation. PloS one, 11(6), p.e0157112.
- [15] Kaggle, Brain Tumor Segmentation dataset [Online]. Available: <https://www.kaggle.com/datasets/nikhilroxtomar/brain-tumor-segmentation> [Accessed Sept. 18, 2025]
- [16] Ronneberger, Olaf, Philipp Fischer, and Thomas Brox. U-net: Convolutional networks for biomedical image segmentation. In International Conference on Medical image computing and computer-assisted intervention, pp. 234-241. Cham: Springer international publishing, 2015
- [17] Lin, Tsung-Yi, Priya Goyal, Ross Girshick, Kaiming He, and Piotr Dollár. Focal loss for dense object detection. In Proceedings of the IEEE international conference on computer vision, pp. 2980-2988. 2017